Chemical interaction, self-ordering and corrosion inhibition properties of 2-mercaptobenzothiazole monolayers: DFT atomistic modelling on metallic copper

Fatah Chiter, Dominique Costa, Vincent Maurice, Philippe Marcus

Chemical interaction, self-ordering and corrosion inhibition properties of 2-mercaptobenzothiazole monolayers: DFT atomistic modelling on metallic copper

Fatah Chiter,* Dominique Costa, Vincent Maurice,* and Philippe Marcus*

PSL University, CNRS – Chimie ParisTech, Institut de Recherche de Chimie Paris/Physical Chemistry of Surfaces Group, 11 rue Pierre et Marie Curie, 75005 Paris, France

E-mail: fatah.chiter@chimieparistech.psl.eu; vincent.maurice@chimieparistech.psl.eu; philippe.marcus@chimieparistech.psl.eu

Abstract

DFT calculations bringing atomic scale insight into the corrosion inhibition properties of 2-mercaptobenzothiazole on copper are reported. Energetic and electronic analysis show that both the thione and thiolate conformers strongly chemisorb on oxide-free Cu(110) surfaces and can self-order to form dense and stable organic barriers saturating all Cu atoms of the topmost metal plane. Increasing monolayer density occurs at the cost of the metal and molecule deformations, but the energy loss is compensated by the layer cohesion energy. The copper vacancy creation energy is higher with thiolate than with thione monolayers, indicating more efficient mitigation of dissolution by adsorbed thiolate.[1]

[1]Preprint accepted for publication in Corrosion Science, 2022. https://doi.org/10.1016/j.corsci.2022.110658

Preprint accepted for publication in Corrosion Science, 2022.
https://doi.org/10.1016/j.corsci.2022.110658

Keywords: Corrosion inhibition, 2-mercaptobenzothiazole, Copper, DFT, Organic Films.

Introduction

Organic molecules are widely used and developed to mitigate the corrosion of metals and alloys in aqueous environments.[1–5] It is well established that what determines the efficiency of the molecules as corrosion inhibitors is their ability to form insoluble organic, organo-metallic or polymeric films on the metal surface that prevent the ingress of aggressive reagents like chloride ions and slow down the dissolution of the metal (or alloy) in the aqueous environment. The corrosion inhibition efficiency thus relies on the stability of the organic film formed on the metal surface and on its physical and/or chemical barrier properties.

For copper and its alloys, organic molecules containing nitrogen, oxygen and sulfur heteroatoms, conjugated double bonds and polar functional groups are frequently used to prevent corrosion in various experimental conditions.[6–18] Among these organic molecules, 2-mercaptobenzothiazole (MBT) has been shown to be very efficient to improve the corrosion resistance of copper in neutral, acidic and alkaline solutions.[19–32] It acts as a mixed type inhibitor mitigating strongly both the cathodic and anodic reactions.[8,28–32] Depending on the oxidized or metallic surface state of copper , MBT interacts with the surface to form monolayer thick films when Cu_2O oxide is stable (pH > 4),[19,20] and multilayer thick films when Cu_2O oxide is unstable (pH < 3),[19,24,31] due to the presence of copper cations.

The Cu substrate may expose oxide-free Cu(hkl) facets, surfaces covered by an intact or defective oxide film, and also dry, hydrated or hydroxylated surface states, which have to be considered to explain the different bonding mechanisms of MBT on copper surfaces. On the oxide free surface, MBT forms an organic layer that prevents Cu(I) oxide formation in alkaline solution.[27,33,34] This has also been observed in the gas phase where MBT, pre-adsorbed on the metallic surface, blocks surface oxidation and oxide growth.[35,36] From

experimental studies, MBT chemisorption on copper surfaces involves the S_{exo} (exo-cyclic) and N atoms.[24,31] In experiments controlled at the atomic scale, the interaction of MBT deposited on the oxide-free Cu(111) surface from the gas phase involves the bonding of S_{exo} and S_{endo} (endo-cyclic) to Cu atoms.[35,36] Other works reported that the bonding of MBT to metallic surfaces, including copper, is through the S_{exo} atom,[22,23] or only via electrostatic interactions.[28]

Density Functional Theory (DFT) calculations, providing atomistic insight into the surface chemistry, have shown that the MBT molecule interacts strongly on oxide-free Cu(111) surfaces and has the ability to self-order and form stable and dense organic layers.[37] The more reactive sites in the MBT molecule are the two sulfur atoms and the NH group or the N atom, depending on the conformer (thione, thiol and thiolate) present in the reactive phase. MBT chemically adsorbed on metallic Cu(111) forms a protective film involving the bonding of the two S atoms.[37] DFT studies also showed that MBT interacts strongly with oxidized and locally de-passivated copper (111) surfaces by the formation of covalent bonds and H-bonds.[38–40] The adsorption behavior of MBT molecule is similar to 2-Mercaptobenzimidazole (MBI) molecule on copper surfaces,[41,42] which can explain the similar efficiency for the two molecules determined experimentally.[19] However, the organic films can be homogeneous or inhomogeneous on the copper surface covered by an intact or defective oxide film, respectively. The molecules in the organic film then adopt different orientation and adsorption configurations.[39,40] The thione (MBTH) species interacts covalently only via the S_{exo} atom with the copper surface covered by an intact oxide film, and the adsorption is enhanced by H-bonding involving the NH group.[39] On copper surfaces covered by a defective oxide film and exposing locally different reactive zones such as metal surface, oxide surface, oxide edges and oxide walls, MBTH adsorption can involve the S_{exo} and S_{endo} atoms or only the S_{exo} atom and the NH group depending on the local reactive zones.[40] For MBT$^{\circ}$ thiolate, adsorption involves the S_{exo} and N atoms independently of the surface states of copper. Both MBT conformers may substitute water and OH groups on the hydrated and hydroxylated

Cu_2O surfaces, respectively.[38,39] Regardless of the copper surface state, the film formed by the MBT thiolate form is the most stable. Depending on specific copper surfaces, the adsorption of thiolate may be more stable than that of thione, like for MBI molecules on Cu(111),[16] on O/Cu(111) and on OH/Cu_2O(111) surface models.[43] In contrast, the thione form is more stable than thiolate on O/Cu_2O(111) and on OH/Cu(111) surface models.[43]

The study of the adsorption strength and configurations of the MBT molecule on oxide-free copper surfaces has shown that its reactivity depends on the Cu(hkl) facets.[44] From DFT calculations performed at low surface coverage, i.e. at low density of the organic monolayer, it has been reported that MBT strongly chemisorbs via the two sulfur atoms on the Cu(220) surface (equivalent to Cu(110)), while it is less strongly bonded on the Cu(200) (equivalent to Cu(100)) and Cu(111) surfaces, in agreement with experimental observations that showed a better protection of oxide-free Cu(110) than of the oxide-free Cu(111) and Cu(100) surfaces at low Cl concentration, which was assigned to the higher chemical activity of the (110) facet.[44]

In the present work, we performed quantum chemical DFT calculations in order to bring deeper atomic scale insight into the adsorption geometry and reactivity of MBT on the Cu(110) surface and the ability of the conformers to self-order and form dense and protective organic films saturating the copper surface. Fig.1 schematizes the adsorption modes of the different MBT species considered for adsorption on the Cu(110) surface from the gas and aqueous phases. The Cu(110) surface is of interest because it enables the introduction of emergent grain boundaries as will be reported separately. In addition, with respect to the most often studied Cu(111) surface, the Cu(110) surface favours the formation of adatoms. Thus, this orientation is of interest for the study of surface defect formation, and the inhibition effect of MBT. We discuss thoroughly the adsorption modes and configurations and the electronic analysis of the thione and thiolate bonding, and their dependence on organic monolayer density (i.e. surface coverage). Adsorption free energies from the aqueous phase of neutral and charged species are also considered with the help of a thermodynamic

cycle. We also performed cross-combined analysis of the adsorption energy and discuss the contributions of the surface and molecule deformation energies, cohesion and desorption energies, and their variation with surface coverage, which is unprecedented for this system. In addition, we performed calculations of the Cu vacancy formation energy in order to better understand the inhibition effect of the molecule on the dissolution of copper.

Computational details

All calculations were performed using the framework of DFT with the periodic plane-wave basis set implemented in Vienna Ab initio Simulation Package (VASP).[45–48] Energy analysis for the reported structures have been obtained with projector-augmented-wave potentials.[49,50] Electron exchange and correlation terms were treated within the generalized gradient approximation (GGA) of Perdew–Burke–Ernzehof (PBE) functional.[51,52] For all calculations, the plane-wave energy cutoff was 450 eV and a Methfessel–Paxton smearing[53] with smearing value of 0.1 eV was used. Atomic positions were relaxed with the conjugate gradient (CG) algorithm until forces on each moving atom were less than 0.02 eVÅ^{-1}. Van der Waals contributions were considered in the Grimme D2 empirical dispersion correction,[54] giving a good compromise for the lattice parameters of copper bulk metal with equilibrium values of 3.57 Å, obtained using a 21×21×21 k-mesh, in good agreement with experimental and theoretical values of 3.61[55] and 3.57 Å,[56] respectively.

A slab with six atomic layers was used for Cu(110) surface, built from copper bulk crystal. We used the unit cell with lateral dimensions of 7.62 and 21.40 Å in $[\bar{1}1\bar{4}]$ and $[2\bar{2}\bar{1}]$ directions, respectively, and allowing to vary the density of the organic monolayer from 0.61 to 3.68 molecules/nm^2. When considering epitaxy relationships, or superstructures formations, the choice of the cell with which the calculations are performed is crucial. In a preceding work, we have envisaged nearly exhaustively the different possible cells for MBT organisation on Cu(111), in which one or two molecules were placed. The most favoured layer density

was 3.5 molecules/nm^2. Another approach consists in taking a large cell and putting more molecules. In our preceding works of MBT adsorption on pre-oxidized Cu, we used a large cell with 9 molecules, also corresponding to the layer density of 3.27 molecules/nm^2. Here, we use the same approach, using a large cell on which 6 molecules can be placed. The calculations conditions are the same as those used in our previous work on Cu(111), PBE corrected with van der Waals corrections. Many other works on this topic are performed with similar calculations conditions.[16,43] The Brillouin zone sampling was set to 3×1×1 k-mesh.[57] The vacuum region was set at more than 18 Å to minimize the interactions in the z direction between periodic images of the system. All calculations were done without any constraint on the structure, except for the two bottom layers of the slab (asymmetric slab). The four upmost metal layers and the molecules were let free to relax.

The isolated molecules were optimised using the same computational conditions, except the Brillouin zone sampling restricted to the Γ-point, in a box with large dimensions of 20Å×20Å×20Å, in the three directions. For the radical MBT° form, spin polarization was implemented to get the energy minimum. The properties of the isolated MBT molecule for different species have been well described by experimental and theoretical studies.[25,37,58–62]

Adsorption from gas phase of neutral MBTH and MBT° species

The adsorption energy of the neutral MBT molecule for the thione (MBTH) and thiolate (MBT°) forms in gas phase was calculated as:

$$E_{\text{ads}} = [E(\text{slab/n-MBT}) - E(\text{slab}) - nE(\text{MBT})]/n \quad (1)$$

where E(slab/n-MBT) is the total energy of the system with MBTH or MBT° adsorbed on the Cu(110) surface. E(slab) and E(MBT) are the energies for the bare relaxed Cu(110) surface and the free MBTH or MBT° species optimized in vacuum, respectively. n is the number of molecules on the surface. The validity of E_{ads} for the thiolate form is limited

to direct adsorption of the species from gas phase to substrate surface (presence of thiolate form in reacting phase), because the thiolate form is considered as energy reference. Hence, It can also be interpreted as binding energy (E_{ads} = - E_{b}) for thiolate form whatever the adsorption mechanism.

Therefore, for the thiolate (MBT°) form, the adsorption energy was also calculated, considering the thione form as the energy reference:

$$E_{\mathrm{ads}} = [E(\mathrm{slab/n\text{-}MBT^{\circ}}) + \frac{n}{2}E(\mathrm{H_2}) - E(\mathrm{slab}) - nE(\mathrm{MBTH})]/n \tag{2}$$

where E(slab/n-MBT°) is the total energy of the system with MBT° adsorbed on the Cu(110) surface from MBTH. $E(\mathrm{H_2})$ is the energy of the released $\mathrm{H_2}$ molecule, optimized in vacuum. The dissociation mechanism of MBTH corresponds to cleavage of the N-H bond and half the H-H bond formation.

Adsorption from gas phase of charged MBT$^-$ species

The equations defined above are limited to the neutral adsorbed species. We avoided using charged species for the calculations due to the employment of periodic boundary conditions. However, the adsorption energy calculated in gas-phase for neutral species can be extended to charged species using a thermodynamic formalism as done in ref.[63] Following this, the adsorption energy for charged species was determined as:

$$E^{\ominus}_{\mathrm{ads}} = E^{\circ}_{\mathrm{ads}} + E^{\circ}_{\mathrm{ea}} - (\phi_{\mathrm{Cu}} + \Delta\phi) \tag{3}$$

where E°_{ea} is the adiabatic electron affinity, calculated as: $E^{\circ}_{\mathrm{ea}} = E(\mathrm{MBT^{\circ}}) - E(\mathrm{MBT^{-}})$ (we follow here the usual convention that E°_{ea} has a positive value). For MBT° the value is 3.76 eV. In the thermodynamic cycle, the electron of MBT- is transferred to the metal, with an energy $-\phi$. ϕ is the surface work function, which can be written as $\phi = \phi_{\mathrm{Cu}} + \Delta\phi$, ϕ_{Cu} is the work function of the clean Cu(110) metal surface, for which we have taken the experimental

value of 4.39 eV.[64,65] $\Delta\phi$ is the work function change induced by the adsorbed molecules, which had to be calculated here. The $\Delta\phi$ values are reported in Table 1 for different surface coverages, adsorption modes and adsorption species.

Table 1: Work function change ($\Delta\phi$ (eV)) induced by the adsorption of thione in -S -S mode and thiolate in -S -N mode on the Cu(110) surface with increasing monolayer density.

	Monolayer density (molecule/nm2)			
	0.61	1.22	2.45	3.68
Thione: -S -S	-1.03	-1.66	-2.17	-2.09
Thiolate: -S -N	-0.39	-0.62	-0.96	-1.26

Adsorption from aqueous phase

In order to account for solvent (water) effects, we used another thermodynamic cycle, as explained in ref.[63,65] Here, we used the free energy G, because it provides a more appropriate thermodynamic potential in aqueous-phase.

For a neutral species, the expression for ΔG_{ads} is:

$$\Delta G_{\text{ads}}^{(\text{aq})} \approx E_{\text{ads}} - \Delta G_{\text{sol}}^{\text{MBT}} + \Delta\Delta G_{\text{sol}}^{\text{MBT//Cu}} \tag{4}$$

where E_{ads} is the adsorption energy of the neutral thione or thiolate species, calculated in the gas phase[2]. $\Delta G_{\text{sol}}^{\text{MBT}}$ is the solvation free energy of the neutral species, and the values for thione and thiolate (radical) species are -0.380 and -0.201 eV, respectively, and correspond to a sum of electronic and zero-point energies calculated by VAPsol.[66,67] These values are close to those calculated using the Polarizable Continuum Model (PCM)[68] and Solvation Model based on Density (SMD)[69] with Gaussian. $\Delta\Delta G_{\text{sol}}^{\text{MBT//Cu}}$ is currently named as differential adsorptive solvation free energy, defined as: $\Delta G_{\text{sol}}^{\text{mol/metal}} - \Delta G_{\text{sol}}^{\text{metal}}$, where the two terms are the solvation free energies of the coated and bare surfaces, respectively.

[2]For adsorption in the gas phase, it is more rigorous to consider ΔG_{ads} than ΔE_{ads}. However, if one considers that $\Delta G_{gas} = \Delta E_{gas} + ZPE + \Delta S_{gas}^{ads}$, our approach is equivalent to neglect the two last terms, which is reasonable as MBT is a rather rigid molecule. Another term that is neglected here is the ΔG of compression from one mole of MBT in the gas phase to the standard concentration of 1 mol.L^{-1} that is used in the liquid phase. This value is however very low and can be neglected.

However, its magnitude is rather small for this type of systems and can be neglected, like for azole molecules on Cu(111),[70] 3-amino-1,2,4-triazole (ATA), benzotriazole (BTAH), and 1-hydroxybenzotriazole (BTAOH) on Cu(111),[63,65] Cu(100)[65] and Cu(110).[65] Therefore, the magnitude of $\Delta G_{\mathrm{ads}}^{(\mathrm{aq})}$ is dominated by the competitive terms between molecule/surface (E_{ads}) and molecule/water ($\Delta G_{\mathrm{sol}}^{\mathrm{MBT}}$) interactions.

For charged species, the corrections from neutral to charged species, which were $E_{\mathrm{ea}}^{\circ} - (\phi_{\mathrm{Cu}} + \Delta\phi)$ in the gas phase, must be considered in the presence of the solvent. The $\Delta\phi^{*}$ term is the work function change of the metal due to an adsorbed thick enough film of liquid water, and its estimated experimentally for Cu(110) as -0.65 eV.[64] To those terms, we add the solvation free energy of the charged thiolate $\Delta G_{\mathrm{sol}}^{\mathrm{MBT}^{-}}$ (-1.164 eV). The expression for ΔG_{ads} is thus:

$$\Delta G_{\mathrm{ads}}^{\ominus(\mathrm{aq})} \approx E_{\mathrm{ads}}^{\ominus} + \Delta\phi - \Delta\phi^{*} - \Delta G_{\mathrm{sol}}^{\mathrm{MBT}^{-}} + \Delta\Delta G_{\mathrm{sol}}^{\mathrm{MBT//Cu}} \tag{5}$$

where $E_{\mathrm{ads}}^{\ominus}$ is the adsorption energy of the charged thiolate species, calculated by Eq.3. $\Delta G_{\mathrm{sol}}^{\mathrm{MBT}^{-}}$ corresponds to a sum of electronic and zero-point energies of MBT^{-}, calculated by VASPsol.[66,67]

The contribution of van der Waals dispersion forces in the adsorption energy was calculated as:

$$E_{\mathrm{vdW}} = [E_{\mathrm{vdW}}(\mathrm{slab/n\text{-}MBT}) - E_{\mathrm{vdW}}(\mathrm{slab}) - nE_{\mathrm{vdW}}(\mathrm{MBT})]/n \tag{6}$$

where E_{vdW}(slab/n-MBT) is the van der Waals energy of the system with MBTH or MBT° adsorbed on the Cu(110) surface. E_{vdW}(slab) and E_{vdW}(MBT) are the van der Waals energies of the bare relaxed Cu(110) surface and the free MBTH or MBT° species optimized in vacuum, respectively.

The cohesion energy in the organic film was calculated as:

$$E_{\mathrm{coh}} = E(\mathrm{n\text{-}MBT}) - nE(\mathrm{MBT}) \tag{7}$$

where E(n-MBT) is the total energy of the organic film, relaxed after separation from the

copper substrate.

The surface deformation energy of the slab was calculated as:

$$E_{\text{deform}}^{\text{slab}} = E^{\text{urlx}}(\text{slab}) - E(\text{slab}) \tag{8}$$

where $E^{\text{urlx}}(\text{slab})$ is the energy of the unrelaxed free slab obtained after separation from the adsorbed molecules.

The molecule deformation energy per molecule in the adsorbed organic layer was calculated as:

$$E_{\text{deform}}^{\text{molecule}} = \sum_{i=1}^{n} \frac{1}{n}[E_i^{\text{urlx}}(\text{MBT}) - E(\text{MBT})] \tag{9}$$

where $E_i^{\text{urlx}}(\text{slab})$ is the energy of one unrelaxed free molecule obtained after adsorption.

The average desorption energy per molecule of thione (MBTH) and thiolate (MBT°) forms was calculated as:

$$E_{\text{des}} = \sum_{i=1}^{n} \frac{1}{n}[E_i(\text{slab/(n-1)-MBT}) + E_i(\text{MBT}) - E(\text{slab/n-MBT})] \tag{10}$$

where E(slab/n-MBT) is the total energy of the system with n adsorbed MBTH or MBT° molecules on the Cu(110) surface. E_i(slab/(n-1)-MBT) and E_i(MBT) are the energies of the $(n-1)$ molecules adsorbed on Cu(110) surface and the free MBTH or MBT° species, respectively. The geometries of "slab/(n-1)-MBT" and "MBT" are the same as in "slab/n-MBT" systems obtained after optimization.

In order to show the ability of MBT inhibitor to slow down the corrosion of the copper surface, we calculated the defect formation energy, which corresponds to the creation of one copper vacancy in the topmost copper plane in the presence and the absence of the inhibitor. The defect formation energy was calculated as:

$$E_f = E_{\text{defect}}(\text{slab/n-MBT}) + E_{\text{Cu}} - E_{\text{perfect}}(\text{slab/n-MBT}) \quad (11)$$

where E_{defect}(slab/n-MBT) and E_{perfect}(slab/n-MBT) are the total energy of the defect and perfect surfaces, respectively, after optimization. E_{Cu} is the energy of bulk copper.

We plotted the charge density difference expressed as follows:

$$\Delta\rho(r) = \rho(r)_{\text{slab/mol}} - (\rho(r)_{\text{slab}} + \rho(r)_{mol}) \quad (12)$$

where $\rho(r)_{\text{slab/mol}}$ is the charge density distribution on the adsorbed system. $\rho(r)_{\text{slab}}$ and $\rho(r)_{\text{mol}}$ are the charge density distributions on the isolated slab and the molecule for the geometry after adsorption, respectively.

Results

MBTH thione chemisorption in -S -S and -S -NH adsorption modes

Figure 2 shows the most stable -S -S and -S -NH adsorption configurations obtained for MBTH monolayers at densities of 2.45 and 3.68 molecule/nm^2 on Cu(110). For the -S -S adsorption mode at surface densities varying from 0.61 to 2.45 molecule/nm^2, the molecules adopt a most stable adsorption configuration similar to the one shown in Figure 2(a). The molecule stands with its plane perpendicular to the copper surface and binds to copper via both sulfur atoms. The sulfur atoms are localized on short bridge sites with S_{exo}—Cu and S_{endo}—Cu bond lengths of 2.30 and 2.25 Å, respectively. At the monolayer density of 3.68 molecule/nm^2 (Figure 2(b)), the most stable adsorption configuration exhibits significant difference. The molecular plane is tilted instead of perpendicular to the copper surface. The S_{exo} atom remains on short bridge site with S_{exo}—Cu bond lengths of 2.25 and 2.30 Å. However, the S_{endo} atom moves from short bridge site at low coverage to top site position at a high monolayer density, with a S_{endo}—Cu bond length of 2.38 Å. At the surface densities

of 2.45 and 3.68 molecule/nm^2, all copper atoms of the topmost plane are bonded to the molecules, meaning that the metal surface is saturated by the organic films. However, the surface coverage of the organic film is of 1 MBTH molecule for 4 Cu atoms and 1 MBTH molecule for 3 Cu atoms, respectively. The molecules are self-assembled and form $\begin{pmatrix} 2 & 0 \\ 1 & 2 \end{pmatrix}$ and $\begin{pmatrix} 2 & 1 \\ -1 & 1 \end{pmatrix}$ superstructures with respect to the substrate unit cell, respectively. This notation is used in surface crystallography to describe superstructures, where the matrix gives the coordinates of the new vectors describing the superstructure with respect to the initial basis set.

The most stable -S -NH adsorption configurations of MBTH obtained at the surface densities of 2.45 and 3.68 molecule/nm^2 are shown in Figures 2(c) and (d), respectively. In contrast to the –S –S adsorption mode, the molecules stand with their plane perpendicular to the surface regardless of the density (from 0.61 to 3.68 molecule/nm^2). The S_{exo} atom and the NH group are directed toward the surface. The S_{exo} atom is localized close to short bridge site, towards the hollow sites of the Cu(110) surface, binding to two Cu atoms with bond length of 2.33 Å. The NH group is localized above a hollow site at the vertical distance of about 1.40 Å from the topmost Cu plane. Like for the -S -S adsorption mode, the molecules form $\begin{pmatrix} 2 & 0 \\ 1 & 2 \end{pmatrix}$ and $\begin{pmatrix} 2 & 1 \\ -1 & 1 \end{pmatrix}$ self-assembled networks with respect to the substrate unit cell at the surface densities of 2.45 and 3.68 molecule/nm^2, respectively. However, in this -S -NH adsorption mode, each molecule binds to only two Cu atoms of the topmost plane. Hence, only $\frac{1}{2}$ and $\frac{2}{3}$ of the topmost Cu atoms are involved in the bonding, respectively.

The adsorption energies calculated using Eq.1 for the most stable configurations are compiled in Table.2. For MBTH in the -S -S adsorption configuration, the adsorption energy is in the same order regardless of surface coverage. The calculated values are -1.95±0.01 eV/molecule for densities from 0.61 to 2.45 molecule/nm^2 and -1.92 eV/molecule for density of 3.68 molecule/nm^2. This means that the densest organic film is the most stable, since more energy is gained per surface area in this case. For MBTH in the -S -NH adsorption mode, the adsorption energy slightly fluctuates between -1.90 and -1.96 eV/molecule for densities

between 0.61 to 2.45 molecule/nm^2 and decreases (in absolute value) by 0.07 eV/molecule at highest surface density. The most dense monolayer is also favored as more energy is gained per surface area. The differences in the adsorption energy values between the -S -S and -S -NH adsorption modes are too small to indicate which organic layer could predominate at a given monolayer density. However, we can conclude that both -S -S and -S -NH adsorption modes are isoenergetic and form the same superstructure at the highest density. This result suggests that the densest organic layer (3.68 molecule/nm^2) could contain a mixture of molecules either in -S -S and -S -NH adsorption mode, or separated domains of molecules adopting one of the adsorption modes. This versatility would give additional configurations entropy, thus further stabilizing the system.

MBT° thiolate chemisorption in -S -S and -S -N adsorption modes

Figure 3 shows the most stable -S -S and -S -N adsorption configurations obtained for MBT° monolayer at densities of 2.45 and 3.68 molecule/nm^2. The -S -S adsorption mode of the thiolate species (Figures 3(a) and (b)) is identical to that of the thione species and the adsorbed molecules form similar superstructure networks. The molecular plane is perpendicular to the copper surface at densities from 0.61 to 2.45 molecule/nm^2 and tilted at the highest monolayer density of 3.68 molecule/nm^2. Both sulfur atoms are involved in the interaction with the surface and all copper surface atoms are involved in the interaction mechanism at the surface densities of 2.45 and 3.68 molecule/nm^2. Regardless of the monolayer density, the S_{exo} atom is localized on short bridge site. The S_{endo} atom is localized on short bridge and top sites at densities from 0.61 to 2.45 molecule/nm^2 and 3.68 molecule/nm2, respectively. The difference in -S -S adsorption configurations between the two conformers lies only in the bond lengths. For the thiolate form, the S_{exo}—Cu bond lengths are shorter by 0.03 Å at densities from 0.61 to 2.45 molecule/nm^2 and both the S_{exo}—Cu and S_{endo}—Cu bond lengths decrease by about 0.06 Å at the density of 3.68 molecule/nm^2, indicating the stronger adsorption of the thiolate form.

Since the adsorption of thiolate can result from the dissociation of the NH group of the thione form on the copper surface "$MBTH_{ads} \longrightarrow MBT^{\circ}_{ads} + \frac{1}{2}H_2$", hence it corresponds to cleavage of the N-H bond and half the H-H bond formation. Thus, we considered the thione form as the reference for the calculation of the adsorption energy using Eq.2. The values, compiled in Table 2, are -1.96, -1.97, -2.09 and -2.06 eV/molecule for densities of 0.61, 1.22, 2.45 and 3.68 molecule/nm^2, respectively, showing a slight variation with increasing monolayer density. These values are close to those found for MBTH in -S -S and -S -NH configurations, meaning that the molecular and dissociative adsorption are isoenergetic. Again, this suggests that the organic monolayer could be either composed of a mixture of dissociatively and molecularly adsorbed molecules, or that separated domain could form at the surface. Note that the barrier for MBTH dissociation to MBT° is not calculated.

The adsorption of the thiolate species can also occur by direct adsorption in the presence of the tautomeric form in the reacting phase. In order to take into account this scenario, we considered the radical thiolate form as the reference for calculating the adsorption energy in Eq.1. The results, reported in brackets in Table 2, show that the adsorption energy is enhanced by 1.60 eV/molecule. This value corresponds to the dehydrogenation of thione into radical thiolate in the vacuum. This means that in the presence of both species in the same reacting phase, the adsorption of thiolate would be favored over that of thione.

The most stable -S -N adsorption configurations of MBT° thiolate obtained at monolayer densities of 2.45 and 3.68 molecule/nm^2 are shown in Figures 3(c) and (d), respectively. For densities from 0.61 to 2.45 molecule/nm^2, the molecular plane is tilted or perpendicular to the copper surface, whereas, at the density of 3.68 molecule/nm^2, all molecules stand perpendicularly. Regardless of the monolayer density, the molecule binds via the same reactive atoms, S_{exo} and N atoms, to similar adsorption sites, short bridge and top sites, respectively. The S_{exo} atom binds covalently to two Cu atoms, with a S_{exo}—Cu bond length ranging from 2.22 to 2.30 Å. The N atom binds covalently to one Cu atom, with a N—Cu bond length ranging from 1.99 to 2.10 Å. At the density of 2.45 molecule/nm^2, the binding of the

organic film involves $\frac{3}{4}$ of the Cu topmost atoms, whereas, at the highest density of 3.68 molecule/nm^2, all Cu atoms of the topmost plane are involved in the adsorption mechanism. The self-assembled monolayer of 2.45 molecule/nm^2 density forms a $\begin{pmatrix} 2 & 0 \\ 1 & 2 \end{pmatrix}$ network, identical to that for the -S -S adsorption mode despite the difference in the adsorption sites of the S_{endo} and N atoms. However, increasing the density to 3.68 molecule/nm^2 leads to a slight distortion of the network formed by the nearest neighbour adsorbed molecules, compared to the perfect $\begin{pmatrix} 2 & 1 \\ -1 & 1 \end{pmatrix}$ arrangement of the -S -S network. In Figure 3(d), we can see that some copper atoms bonded to N atom moves laterally from their initial position, leading to a slight reconstruction of the Cu(110) topmost plane. As a consequence, the formed network corresponds to a distorted $\begin{pmatrix} 2 & 1 \\ -1 & 1 \end{pmatrix}$ superstructure.

As in the case of the -S -S adsorption mode, we calculated the adsorption energy considering the thione (Eq.2) or thiolate (Eq.1) species as reference (Table 2). For adsorption by dissociation of the thione form on the copper surface, the adsorption energy is -2.29±0.01 eV/molecule at densities from 0.61 to 2.45 molecule/nm^2 and it decreases (in absolute value) by 0.20 eV/molecule (E_{ads} = -2.09 eV/molecule) at the density of 3.68 molecule/nm^2. However, the adsorption remains strong regardless of the density and the energy gain per surface area is favourable to the formation of the most dense film (Table 2). Considering the direct adsorption of the thiolate form from the reacting phase (a possible scenario at high pH[71]) the values are -3.90±0.01 and -3.70 eV/molecule at densities from 0.61 to 2.45 and 3.68 molecule/nm^2, respectively. The results confirm that, for the -S -N adsorption mode, thiolate adsorption is also favored when considering the competitive adsorption of the thione and thiolate forms present in the same reacting phase.

Adsorption of charged thiolate (MBT^-) species

The adsorption energy of the charged thiolate (MBT^-) species, in the -S -N adsorption mode, calculated using Eq.3, is reported in Table 2 for different monolayer densities. For comparison, the radical thiolate (MBT°) adsorption energies, calculated with Eq.2 and using

the thione form as the reference energy, are also reported. The values are plotted in Fig.4a for both the radical (MBT°) and the charged (MBT^{-}) thiolate species in -S -N adsorption mode and for MBTH.

The results reveal that the adsorption process of the charged species on the Cu(110) surface is exothermic for all monolayer densities, as found for the neutral species. However, at low density, the adsorption of the charged form is more exothermic than that of the neutral form by 0.31 eV, and the trend is reversed at high density, i.e. the adsorption of the neutral form is more favorable than that of the charged species by 0.56 eV. This is due to the fact that the work function at low coverage remains larger than the electron affinity of thiolate species (remember that those values are introduced in the equations to recover the E_{ads} of the charged species). At high coverage (surface density of 2.45 molecule/nm^2 and above), the work function change induced by the adsorbed molecules reduces strongly the metal work function of Cu(110) and the electron affinity of the molecule becomes larger than the work function of the Cu(110)/MBT system, which favors the adsorption of the radical species. Indeed, the work function change induced by the adsorbed molecules depends on the monolayer density (Table.1), and it decreases from -0.39 eV to -1.26 eV with increasing density from 0.61 molecule/nm^2 to 3.68 molecule/nm^2, respectively. Another important point revealed by considering the charged species is that at higher (3.68 molecule/nm^2) monolayer density, the adsorption of the thione form is more exothermic by 0.39 eV/molecule than charged thiolate species, and the neutral thiolate form is more favored than the thione form by 0.17 eV/molecule.

Adsorption from aqueous phase of different MBT species

The results for the adsorption from aqueous phase are reported in Table.2 and compiled in Fig.4b. For neutral molecules, they reveal a similar adsorption behavior in aqueous solution as in the gas phase. The adsorption of the two neutral forms is exothermic. For the trend found in the gas phase to be reversed, it is necessary that $\Delta G_{\text{ads}}^{(\text{aq})}(\text{MBTH}) -$

$\Delta G_{\text{ads}}^{(\text{aq})}(\text{MBTH}^{\circ}) < 0$. To satisfy this condition, first, the solvation free energy of the radical neutral species (MBT°) has to be higher (in absolute value, thus more soluble) than the solvation free energy of neutral species ($\Delta G_{\text{sol}}^{\text{MBT}^{\circ}} - \Delta G_{\text{sol}}^{\text{MBTH}} < 0$) and, second, the difference between the solvation free energies of the two species must be larger than the difference between their adsorption energies calculated in gas phase ($\Delta G_{\text{sol}}^{\text{MBT}^{\circ}} - \Delta G_{\text{sol}}^{\text{MBTH}} < E_{\text{ads}}(\text{MBT}^{\circ}) - E_{\text{ads}}(\text{MBTH})$). This is not the case here, the solvation free energy of MBT° (-0.19 eV) is lower than that of MBTH (-0.35 eV), meaning that MBTH is more easily solvated than MBT°. In addition, the adsorption energy difference is about -0.33 eV/molecule for monolayer densities of 0.61 to 2.45 molecule/nm^2, and of -0.17 eV/molecule for 3.68 molecule/nm^2. For all these reasons the thiolate radical form remains more stable than the thione form also when considering adsorption from an aqueous solution. The adsorption behavior for a charged species (MBT^{-}) is completely different. The adsorption of a charged species in aqueous solution is less favorable than the adsorption of the neutral species, due to a strong solvation energy of the anion. The adsorption energy calculated in water is lower than that calculated in gas phase. However, the adsorption of the charged species remains exothermic at all surface coverages.

Electronic analysis

The type of bonding formed at the molecule/surface interface is well described by the electronic analysis, using Eq.12. Figure 5 shows the charge density difference ($\Delta\rho$) plots for the thione in -S -S and -S -NH adsorption modes at densities from 0.61 to 2.45 molecule/nm^2 (snapshots (a) and (c)) and 3.68 molecule/nm^2 (snapshots (b) and (d)). The chemisorption of the molecule via S_{exo}—Cu and S_{endo}—Cu covalent bonds is confirmed in Figures 5(a) and (b) by the charge density accumulation (light blue color) between the sulfur atoms and the Cu atoms involved in the interaction, in agreement with the measured S—Cu bond lengths. For -S -NH adsorption configuration, Figure 5(c) and (d) confirm the S_{exo}—Cu covalent bonding. In this case, the adsorption of the molecule is enhanced by electrostatic interac-

tions between the NH group and the hollow site of the Cu(110) surface. Furthermore, the $\Delta\rho$ plot shows an H-bond between N-H and Cu. Such H-bonds with copper are known.[72] The charge density difference ($\Delta\rho$) plots for the thiolate from in -S -S and -S -N adsorption modes are shown in Figure 6. For the -S -S adsorption mode at densities varying from 0.61 to 2.45 and of 3.68 molecule/nm^2, shown in Figures 6(a) and (b), respectively, the bonding is provided by S_{exo}—Cu and S_{endo}—Cu covalent bonds, which confirms that the preferred adsorption sites on the surface are similar to those involved in -S -S adsorption modes of thione form. We can see that the iso-surface is slightly larger for the thiolate form, in agreement with shorter S—Cu bond lengths. For the -S -N adsorption mode at densities varying from 0.61 to 2.45 and of 3.68 molecule/nm^2, shown in Figures 6(c) and (d), respectively, both the S and N atoms of the molecule are involved in a covalent interaction with the Cu atoms. However, the iso-surface shows that the contribution to the bonding is dominated by the S_{exo}—Cu covalent bond (larger iso-surface) rather than by the N—Cu covalent bonding (less dense iso-surface).

Discussion

Our results confirm the strong reactivity of sulfur atoms toward copper, especially the S_{exo} atom. The deprotonation of the NH group of the thione form to give thiolate makes the N atom of the molecule more reactive, which enhances the adsorption strength of the molecule. At low monolayer density, when only the molecule-surface interaction drives the adsorption, we thus have the following ranking in the interaction with the surface: -S -N $>$ -S -S $\simeq$ -S -NH. This trend agrees with that found on the Cu(111) surface, the adsorption energies on the Cu(111) surface being lower.[37] Regarding the self-assembly properties, we find that the –S –S configurations adopt a tilted structure at high coverage, whereas the -S –N(H) ones are perpendicular. At high density, steric hindrance and molecule deformation can explain why the perpendicular adsorption mode is favored (which is further discussed below).

We have also seen that the -S -S and -S -NH adsorption modes of the thione conformer are isoenergetic. This suggests the possible formation of separated domains at the surface as well as domains mixing both adsorption modes, which would bring mixing entropy and thus additional stability to the organic layer. For the thiolate conformer, the -S -N adsorption mode is the most stable at densities from 0.61 to 2.45 molecule/nm^2, but at the highest density of 3.68 molecule/nm^2, the -S -S and -S -N configurations are isoenergetic, suggesting also the possibility of mixed adsorption. At high density of the organic monolayer, thiolate adsorption is always favored compared to thione adsorption whatever the adsorption mode, particularly when adsorbed directly from the reactive phase. We can also note that, for both conformers and for a given adsorption mode, the adsorption energy per molecule is only weakly dependant on the density of the organic monolayer. This can be due to the absence of interaction between the molecules in the film or to the combination of opposite trends. This is examined in details in the following.

Cohesion and deformation energies

In order to better understand why the adsorption energy shows only slight fluctuations with the density of the organic layer, and even slightly decreases in absolute value (less exothermic adsorption) for thiolate in -S -N mode at the highest density of 3.68 molecule/nm^2, we decomposed the adsorption energy in two terms ($E_{\mathrm{ads}} = E_{\mathrm{vdW}} + E_{\mathrm{DFT}}$). The first term ($E_{\mathrm{vdW}}$, calculated using Eq.6) corresponds to the contribution of van der Waals dispersion forces between the molecules and the surface, and the second (E_{DFT}) relates to the chemical, covalent bonding of the molecule with the copper surface. This decomposition, shown in Figure 7 for thione and thiolate species, reveals that increasing the density of the organic film and thus the surface coverage increases the contribution of E_{vdW} and decreases that of E_{DFT}.

Figure 8 shows the variation of the cohesion energy (E_{coh}) with increasing density of the organic monolayers, as calculated using Eq.7. This variation, similar to that of the dispersion

forces (E_{vdW} term), reveals that the denser the organic layer, the stronger the molecule-molecule interactions in the film. At densities of 0.61 and 1.22 molecule/nm^2, the molecules are not close enough to interact, as demonstrated by a weak cohesion energy in the organic layer. The cohesion energy becomes significant at the higher densities of 2.45 and 3.68 molecule/nm^2. Figure 8 also shows a stronger cohesion energy in the organic thiolate layer than in the thione layer. Besides, the distance between the rings is superior to 3.6 Å, it is 4.4 Å at high coverage and longer at low surface coverage. Thus, the cohesion energy does not reflect a $\pi - \pi$ interaction. The interaction between the aromatic rings is dominated by vdW contributions.

Let us examine the former case in more details. At the intermediate density of 2.45 molecule/nm^2 (Figure 3(c)), all MBT° molecules stand parallel to each other, with the S atom bridging two Cu atoms in nearest neighbour position. Thus, all Cu atoms in a close-packed row are bonded to a S atom. In the next close-packed row, $\frac{1}{2}$ of Cu atoms are bonded to N atoms. At the highest density of 3.68 molecule/nm^2 (Figure 3(d)), a bridging S atom now alternates with a N atom in near on-top position along all Cu close-packed rows. Whereas the molecules were perfectly aligned following the Cu close-packed rows at 2.45 molecule/nm^2 (Figure 3(c)), some steric hindrance appears now in the organic film and the additional molecules are distorted (Figure 3(d)). The intra molecular bond lengths remain typical of the molecules but the molecules are not planar anymore, with a distortion of some degrees from the dihedral angle in the molecular cycle (Figure 3(d)). The consequence of this distortion is that each individual molecule is less stable and has a higher energy compared to the free molecule, and thus the distorted molecules are more stabilized by their interactions with the metal. As for the metal, we observe that some Cu atoms bonded to N atoms are displaced from their initial position (Figure 3(d)). In average, every nine Cu atom of the close-packed rows is displaced by the molecular arrangement. The Cu atoms to which N is bonded are also slightly extruded from the surface. Thus, all Cu atoms of the topmost plane are involved in the –S –N bonding of MBT° thiolate, and this high density is obtained at

the cost of metal surface and molecule deformation energies.

Figure 9 shows the variation of the deformation energies of the metal surface, calculated using Eq.8, and of the molecule, calculated using Eq.9, with increasing density of the thione and thiolate monolayers, respectively. For the thiolate in -S -N adsorption mode at the highest density of 3.68 molecules/nm^2, the calculated deformation energy of the metal plane is 1.65 eV for the cell containing 6 molecules, which corresponds to 0.27 eV of surface deformation per adsorbed molecule. All factors put together, the adsorption energy is only slightly lower (0.2 eV) than at lower densities of the organic film. This means that the energy gain per surface area will be the highest for the most dense film, which plays in favour of the formation of a denser film. Note that, in this case, this is possible thanks to the molecule and metal surface deformations. Such a deformation effect is less significant for the adsorbed -S -S thiolate configuration, where the metal surface deformation energy is weak. The molecules have similar deformation energy (0.3 eV), but the -S -S adsorption being less exothermic than the -S -N one, finally, the lower deformation cost compensates the lower bond formation gain, and the -S -S and -S -N thiolate configurations are isoenergetic.

Let us emphasize that we evidence here complex relationships between adhesion strength, and molecule and metal surface deformation energy that render the adsorption mechanisms difficult to predict without a detailed analysis of each system. However, one remark can be done when comparing the present results with those obtained on the Cu(111) surface.[73] On the more compact Cu(111) surface, no surface deformation was observed, as there are more sites to accommodate the bonding of the adsorbate, and as the stability of the surface atoms is higher.[73] It was already pointed out that open surfaces Cu(110) and Cu(100) surfaces allow easier defects formation than on the Cu(111) one,[73] a trend in line with the present results.

Figure 8 also shows that, for a given organic monolayer density, the cohesion energy values are close (within 0.1 eV/molecule) for the MBTH thione form in -S -S and -S -NH adsorption modes, whereas, for the MBT° thiolate form, the organic layer in -S -S adsorption mode

exhibits a higher cohesion energy than in -S -N adsorption mode (by 0.22 eV/molecule for a density of 3.68 molecule/nm^2). This is due to the tilted orientation of the molecules in the -S -S configuration. From the analysis of dispersion forces in the adsorption mechanism, we can thus conclude that the molecule/molecule and molecule/surface interactions contribute to stabilize the organic film with increasing density. The decrease (in absolute value) or the slight variation observed on the adsorption energy with increasing surface coverage can be due to the contribution of other energy terms, which results in mutual cancellation with the dispersion energy contribution.

Regarding the second term E_{DFT}, Figure 7 shows that it decreases (in absolute value) when the surface density of the organic film increases and thus that it is responsible for the decrease of the adsorption energy. This loss in the chemical bonding with increasing monolayer density can be assigned to the deformation of both the organic film and the surface substrate. As seen in Figure 9 for the thione and thiolate forms, increasing the surface coverage to form denser organic films increases the deformation energies of the molecule in the organic films and of the metal surface. In addition, we can see that the deformation energy is more significant for the thiolate form than for the thione form, meaning that the thiolate form loses more adsorption energy, particularly in the -S -N adsorption configuration. Thus, a larger deformation energy implies a more significant loss in the adsorption energy.

Desorption energy

Figure 10 shows the variation of the desorption energy, calculated using Eq.10, for one thione and thiolate molecule in -S -S or -S -NH (-S -N) adsorption mode as a function of the density of the organic films. Note that a more positive desorption energy refers to a stronger adsorption and a more negative adsorption energy. It is clearly observed that increasing the organic film density increases the desorption energy for both species and for each adsorption mode. Since a higher desorption energy implies a stronger bonding of the molecule to the surface, these results reveal that the molecule in a denser organic film is more strongly bonded

to the copper surface than in a less dense organic layer, which confirms the formation of dense organic films on the Cu(110) surface. Indeed, when the film density varies from 0.61 to 3.68 molecule/nm^2, the desorption energy increases by 0.26 and 0.22 eV/molecule for the thione form in -S -S and -S -NH adsorption mode, respectively, and by 0.38 and 0.41 eV/molecule for the thiolate form in -S -S and -S -N adsorption modes, respectively. In contrast to the adsorption energy that shows slight variation with increasing surface coverage, the adsorption energy normalized to unit area shows clearly that the formation of a dense organic monolayer is favored (Table 2). We recall that the main reason to obtain close adsorption energy values at different monolayer densities was that the deformation energies of the molecule and metal surface increase with increasing density, which reduces significantly the contribution of the chemical interaction term (E_{DFT}) in the adsorption energy.

Another point to emphasize relates to the adsorption modes of the molecule on the Cu(110) surface. The thione form shows no significant difference of desorption energy for the -S -S and -S -NH adsorption modes, with an energy difference ranging from 0.03 to 0.1 eV depending on adsorption density. This result confirms the conclusion drawn from the analysis of the adsorption energy that both adsorption modes of the thione form may coexist on the Cu(110) surface at different surface coverages. In contrast, for the thiolate form, the desorption energy shows clearly that the -S -N adsorption mode is more stable than the -S -S adsorption mode, whatever the adsorption density. The energy difference between the two is 0.36 eV for a density of 0.61 and 1.22 molecule/nm^2, 0.15 eV for 2.45 molecule/nm^2 and 0.39 eV for 3.68 molecule/nm^2. This information was not obtained by analysis of the adsorption energy at the highest density of 3.68 molecule/nm^2 that showed that both adsorption modes are isoenergetic, due on one hand to the higher deformation energy and on other hand to the higher cohesion energy of the -S -N adsorption mode.

This analysis of the trends of the adsorption, deformation and desorption energies evidences that both forms of the MBT molecule will tend to form dense organic films on the Cu(110) surface, thus providing a protection barrier against corrosion of copper. Among all adsorption

configurations studied in this work, we find that the thione form can adsorb in both -S -S and -S -NH modes, leading to the formation of an inhomogeneous organic layer on the copper surface, which may lead to the coexistence of different domains on the surface. In contrast, the thiolate species can adsorb preferentially in the -S -N configuration, leading to the formation of an homogeneous organic film. The results also reveal that the adsorption of the radical thiolate form is slightly favored over that of the thione form, considering the deprotonation of thione to thiolate on the Cu(110) surface. However, with both forms present in the same reacting phase, considering that the MBT pKa is 6.9,[71,74] the competitive adsorption clearly favors the radical thiolate form regardless of the density of the organic film. For charged thiolate species in solvent (water), its adsorption on Cu(110) surface remains exothermic, but less favored than thione form.

Defect formation energy

In order to study the ability of the adsorbed molecule to mitigate the dissolution of copper, we calculated the defect formation energy using Eq.11. This quantity (E_f) corresponds to the energy required to create one copper vacancy in the substrate topmost plane. The higher the value, the more difficult the extraction of copper and thus the more resistant the surface against dissolution. Calculations were performed for the bare Cu(110) surface, giving a reference value of 0.33 eV, and for the Cu(110) surface covered with the thione and thiolate monolayers with the adsorption modes and densities discussed above. The results, compiled in Table.3, show that both adsorption modes of the thione enhance the stability of the copper surface, with only slight variations in the defect formation energy according to the molecule reactive sites. All copper atoms covalently bonded to the S_{exo} atom are stabilized by the adsorption of the molecule. The defect formation energy ranges from 0.50 to 0.68 eV, depending on the adsorption mode and monolayer density. This result reveals that the S_{exo} atom in the MBT thione form plays the predominant role to mitigate the dissolution of the copper surface.

At low monolayer density, the copper atoms not involved in the adsorption mechanism of the thione form and those interacting with the S_{endo} atom in the -S -NH adsorption mode have a defect formation energy similar to that of the copper atoms of the bare Cu(110) surface, and those interacting with -NH group in the -S -NH adsorption mode are stabilized by only 0.07 eV. In contrast, at high monolayer density, all copper surface atoms are stabilized by the adsorption of the organic layer. The copper atoms interacting with the S_{endo} atom or -NH group in the -S -S or -S -NH adsorption modes, respectively, are also stabilized by the presence of the organic layer since the calculated defect formation energy increases to 0.52 and 0.50 eV, respectively (Table.3). This indicates the local nature of the protection effect against corrosion of the copper surface.

Since the -S -N adsorption mode of the thiolate form is preferred on the Cu(110) surface, we focus the analysis of the defect formation energy on this adsorption mode only. Table.3 shows that both the S_{exo} and N atoms of the MBT thiolate play the predominant role to mitigate the corrosion of copper by enhancing the stability of all copper surface atoms involved in the interaction with the molecule. The defect formation energy obtained with the thiolate film is higher than that obtained with the thione film, indicating that the thiolate form provides better barrier protection.

At low monolayer density, the copper atoms not involved in the adsorption mechanism remain unprotected against dissolution with a defect formation energy of 0.33 eV equal to that on the bare Cu(110) surface. This confirms that the protection effect of the molecule is local and that the good corrosion inhibitor properties of the MBT molecule relates to its ability to form a dense organic layer saturating all copper surface atoms. For the two copper atoms interacting with the S_{exo} atom of adsorbed thiolate, the defect formation energy is 0.80 and 0.65 eV, higher than for the adsorbed thione. The copper atom interacting with the N atom also shows higher stability, with a defect formation energy of 0.95 eV.

At high surface coverage, all copper surface atoms are stabilized by the adsorption of the thiolate. The defect formation energies are 0.60 and 0.70 eV for the two copper atoms

interacting with S_{exo} atom, of the same order to those found for the copper atoms involved in the bonding with the S_{exo} atom of the thione form. As the adsorption of the thiolate form at highest density involves the reconstruction of some of the copper surface atoms interacting with the N atom (Figure 3(d)), different defect formation energy of copper vacancies were calculated. The defect formation energy is 0.58 eV for the non-displaced copper atom, and 1.08 eV for the displaced copper atom. The values remain high despite the surface reconstruction, indicating that the stability of the all copper atoms is enhanced by the formation of the thiolate monolayer saturating the surface.

Conclusion

The reported DFT calculations show that the MBTH thione conformer can competitively adsorb on the Cu(110) surface in (i) -S -S mode via its two sulfur atoms covalently bonded to short bridge and top sites, and (ii) in -S -NH mode via S_{exo}–Cu covalent bonding on short bridge site and electrostatic interaction of the NH group on hollow site. In contrast, the MBT° thiolate conformer preferentially adsorbs in -S -N mode via the S_{exo} and N atoms covalently bonded to short bridge and top sites, respectively. At saturation of the metal surface corresponding to a density of the organic monolayer of 3.68 molecule/nm^2, the molecules form self-ordered networks with all Cu atoms involved in the bonding interaction. Some of the Cu atoms bonded to N atoms are displaced to facilitate the self-organization of molecules. Analysis of the energetic trends confirms the strong adsorption of the conformers present in gas or aqueous phases, and the ability of the molecules to form self-ordered organic barrier film of the highest density on the Cu(110) surface. The thione monolayer may be composed of both -S -S and -S -NH chemisorption modes, while the thiolate monolayer is homogeneous and dominated by the -S -N chemisorption mode. The adsorption trend of neutral species is similar in gas and aqueous phases. Despite the strong solvation energy of the charged species, its adsorption remains exothermic in aqueous solution.

For the high density monolayer we observe a balance between the metal-molecule interaction, cohesion in the layer and energy cost of metal surface and molecule deformations. The calculation of the desorption energy shows that the molecule in the denser organic film is strongly bonded to the copper surface.

Calculation of the vacancy formation energy in the topmost Cu plane evidences the local effect of the organic monolayers for enhancing the stability of the copper atoms involved in the adsorption mechanism, thus confirming that corrosion inhibition properties result from the ability of the molecules to form dense organic layer strongly adsorbed and saturating all metal surface atoms. Vacancy formation energy is higher with thiolate than with thione monolayers, indicating that thiolate would provide better protection to the copper surface against dissolution. Both S_{exo} and N atoms of the adsorbed thiolate conformer play the predominant role to make this species an efficient corrosion inhibitor of the copper metallic surface.

The formation of a dense layer of molecule on the surface provides a physical barrier against the penetration of aggressive species and their interaction with the metal surface. Also, the bonding of the molecular layer involves all Cu surface atoms, thus no available adsorption site remains at the surface. Moreover, the defect formation energy is higher in presence of the adsorbed molecular layer. All these facts suggest that MBT is an anodic inhibitor. Besides, this dense layer may also inhibit the adsorption of dioxygen or proton that are the most common reactants of the cathodic reaction.

Data availability statement

The data that support the finding of this study are available from the corresponding authors upon reasonable request.

Author contributions

F. Chiter: Methodology; Validation; Investigation; Formal analysis; Visualization; Writing—Original Draft; Writing—Review Editing.

D. Costa: Resources; Supervision; Writing—Review Editing.

V. Maurice: Supervision, Writing—Review; Editing Funding acquisition.

P. Marcus: Supervision; Writing—Review and Editing; Funding acquisition Project management.

Declaration of Competing Interest

The authors declare that they have no known competing financial interests or personal relationships that could have appeared to influence the work reported in this paper.

Acknowledgement

This project has received funding from the European Research Council (ERC) under the European Union's Horizon 2020 research and innovation program (ERC Advanced Grant No.741123, Corrosion Initiation Mechanisms at the Nanometric and Atomic Scales: CIMNAS).

The authors thank GENCI for high performance calculations in the national (CINES) center under the A0040802217.

References

(1) Twite, R. L.; Bierwagen, G. P. Review of alternatives to chromate for corrosion protection of aluminum aerospace alloys. Prog. Org. Coat. **1998**, 33, 91–100.

(2) Sinko, J. Challenges of chromate inhibitor pigments replacement in organic coatings. Prog. Org. Coat. **2001**, 42, 267–282.

(3) Raja, P. B.; Sethuraman, M. G. Natural products as corrosion inhibitor for metals in corrosive media - A review,. Mater. Lett. **2008**, 62, 113–116.

(4) Gece, G. Drugs: A review of promising corrosion inhibitors. Corros. Sci. **2011**, 53, 3873.

(5) Gangopadhyay, S.; Mahanwar, P. A. Recent developments in the volatile corrosion inhibitor (VCI) coatings for metal: A review. J. Coat. Technol. Res. **2018**, 15, 789–807.

(6) Musiani, M. M.; Mengoli, G. An electrochemical and SERS investigation of the influence of pH on the effectiveness of some corrosion inhibitors of copper. J. Electroanal. Chem. **1987**, 217, 187–202.

(7) Subramanian, R.; Lakshminarayanan, V. Effect of adsorption of some azoles on copper passivation in alkaline. Corros. Sci. **2002**, 44, 535–554.

(8) Zhang, D.; xin Gao, L.; ding Zhou, G. Inhibition of copper corrosion in aerated hydrochloric acid solution by heterocyclic compounds containing a mercapto group. Corros. Sci. **2004**, 46, 3031–3040.

(9) Tan, Y. S.; Srinivasan, M. P.; Pehkonen, S. O.; Chooi, S. Y. M. Effects of ring substituents on the protective properties of self-assembled benzenethiols on copper. Corros. Sci. **2006**, 48, 840–862.

(10) Antonijevic, M. M.; Petrovic, M. B. Review copper corrosion inhibitors. a review. Int. J. Electrochem. Sci. **2008**, 3, 1.

(11) Niamien, P. M.; Essy, F. K.; Trokourey, A.; Yapi, A.; Aka, H. K.; Diabate, D. Correlation between the molecular structure and the inhibiting effect of some benzimidazole derivatives. Mater. Chem. Phys. **2012**, 136, 59–65.

(12) Tao, Z.; He, W.; Wang, S.; Zhou, G. Electrochemical Study of Cyproconazole as a

Novel Corrosion Inhibitor for Copper in Acidic Solution. Ind. Eng. Chem. Res. **2013**, 52, 17891–17899.

(13) Finšgar, M. 2-Mercaptobenzimidazole as a copper corrosion inhibitor: Part I. Long-term immersion, 3D-profilometry, and electrochemistry. Corros. Sci. **2013**, 72, 82–89.

(14) Finšgar, M. 2-Mercaptobenzimidazole as a copper corrosion inhibitor: Part II. Surface analysis using X-ray photoelectron spectroscopy. Corros. Sci. **2013**, 72, 90–98.

(15) Milošev, I.; Kovačević, N.; Kovač, J.; Kokalj, A. The roles of mercapto, benzene and methyl groups in the corrosion inhibition of imidazoles on copper: I. Experimental characterization. Corros. Sci. **2015**, 98, 107–118.

(16) Kovačević, N.; Milošev, I.; Kokalj, A. The roles of mercapto, benzene, and methyl groups in the corrosion inhibition of imidazoles on copper: II. Inhibitor–copper bonding. Corros. Sci. **2015**, 98, 457–470.

(17) Qiang, Y.; Zhang, S.; Yan, S.; Zou, X.; Chen, S. Three indazole derivatives as corrosion inhibitors of copper in a neutral chloride solution. Corros. Sci. **2017**, 126, 295–304.

(18) A. Fateh, M. A.; Rezvanian, A. R. Review of corrosive environments for copper and its corrosion inhibitors. Arabian J. Chem. **2020**, 13, 1481,.

(19) Chadwick, D.; Hashemi, T. Electron spectroscopy of corrosion inhibitors: Surface films formed by 2-mercaptobenzothiazole and 2-mercaptobenzimidazole on copper. Surf. Sci. **1979**, 89, 649–659.

(20) Ohsawa, M.; Suetaka, W. Spectro-electrochemical studies of the corrosion inhibittion of copper by 2-mercaptobenzothiazole. Corros. Sci. **1979**, 19, 709–722.

(21) He, D.; Chen, F.; Chen, J.; Yao, S.; Wei, W. Real-time bulk acoustic wave studies of the inhibition behavior of mercaptobenzothiazole on copper. Thin Solid Films **1999**, 352, 234–238.

(22) Woods, R.; Hope, G. A.; Watling, K. A SERS spectroelectrochemical investigation of the interaction of 2-mercaptobenzothiazole with copper, silver and gold surfaces. J. Appl. Electrochem. **2000**, 30, 1209–1222.

(23) Tan, Y. S.; Srinivasan, M. P.; Pehkonen, S. O.; Chooi, S. Y. M. Self-assembled organic thin films on electroplated copper for prevention of corrosion. J. Vac. Sci. Technol. A **2004**, 22, 1917.

(24) Kazansky, L. P.; Selyaninov, I. A.; Kuznetsov, Y. I. Adsorption of 2-mercaptobenzothiazole on copper surface from phosphate solutions. Appl. Surf. Sci. **2012**, 258, 6807–6813.

(25) Li, J.; Du, C. W.; Liu, Z. Y.; Li, X. G.; Liu, M. Inhibition Film Formed by 2-mercaptobenzothiazole on Copper Surface and Its Degradation Mechanism in Sodium Chloride Solution. Int. J. Electrochem. Sci. **2016**, 11, 10690–10705.

(26) Grekulović, V.; Vujasinović, M. R.; Mitovski, A. Electrochemical Behavior of AgCu50 in Alkaline Media in the Presence of Clorides and 2-mercaptobenzothiazole. J. Min. Metall. Sect. B-Metall **2017**, 53, 349–356.

(27) Chen, Y.-H.; Erbe, A. The multiple roles of an organic corrosion inhibitor on copper investigated by a combination of electrochemistry-coupled optical in situ spectroscopies. Corros. Sci. **2018**, 145, 232–238.

(28) Shahrabi, T.; Tavakholi, H.; Hosseini, M. G. Corrosion inhibition of copper in sulphuric acid by some nitrogen heterocyclic compounds. Anti-Corrosion Methods and Materials **2007**, 54, 308–313.

(29) Marconato, J. C.; Bulho, L. O. A spectroelectrochemical study of the inhibition of the electrode process on copper by 2- mercaptobenzothiazole in ethanolic solutions. Electrochim. Acta **1998**, 43, 771–780.

(30) Bao, Q.; Zhang, D.; Wan, Y. 2-Mercaptobenzothiazole doped chitosan/11-alkanethiolate acid composite coating: Dual function for copper protection. Appl. Surf. Sci. **2011**, 257, 10529–10534.

(31) Finšgar, M.; Merl, D. K. An electrochemical, long-term immersion, and XPS study of 2-mercaptobenzothiazole as a copper corrosion inhibitor in chloride solution. Corros. Sci. **2014**, 83, 164–175.

(32) Ramírez-Cano, J. A.; Veleva, L.; Souto, R. M.; Fernández-Pérez, B. M. SECM study of the pH distribution over Cu samples treated with 2-mercaptobenzothiazole in NaCl solution. Electrochem. commun. **2017**, 78, 60–63.

(33) Sharma, S. B.; Maurice, V.; Klein, L. H.; Marcus, P. Local Inhibition by 2-mercaptobenzothiazole of Early Stage Intergranular Corrosion of Copper. Journal of The Electrochemical Society **2020**, 167, 162504.

(34) Sharma, S. B.; Maurice, V.; Klein, L. H.; Marcus, P. Local Effects of Organic Inhibitor Molecules on Passivation of Grain Boundaries Studied In Situ on Copper. Journal of The Electrochemical Society **2021**, 168, 061501.

(35) Wu, X.; Wiame, F.; Maurice, V.; Marcus, P. Adsorption and thermal stability of 2-mercaptobenzothiazole corrosion inhibitor on metallic and pre-oxidized Cu(111) model surfaces. Appl. Surf. Sci. **2020**, 508, 145132.

(36) Wu, X.; Wiame, F.; Maurice, V.; Marcus, P. 2-Mercaptobenzothiazole corrosion inhibitor deposited at ultra-low pressure on model copper surfaces. Corros. Sci. **2020**, 166, 108464.

(37) Vernack, E.; Costa, D.; Tingaut, P.; Marcus, P. DFT studies of 2-mercaptobenzothiazole and 2-mercaptobenzimidazole as corrosion inhibitors for copper. Corros. Sci. **2020**, 174, 108840.

(38) Chiter, F.; Costa, D.; Maurice, V.; Marcus, P. A DFT-based Cu(111)||Cu_2O(111) model for copper metal covered by ultrathin copper oxide: structure, electronic properties and reactivity. J. Phys. Chem. C **2020**, 124, 17048–17057.

(39) Chiter, F.; Costa, D.; Maurice, V.; Marcus, P. DFT investigation of 2-mercaptobenzothiazole adsorption on model oxidized copper surfaces and relationship with corrosion inhibition. Appl. Surf. Sci. **2021**, 537, 147802.

(40) Chiter, F.; Costa, D.; Maurice, V.; Marcus, P. Corrosion inhibition of locally de-passivated surfaces by DFT study of 2-mercaptobenzothiazole on copper. npj Materials Degradation **2021**, 5, 52.

(41) Chiter, F.; Costa, D.; Maurice, V.; Marcus, P. Atomic Scale Insight into Corrosion Inhibition: DFT Study of 2- Mercaptobenzimidazole on Locally De-Passivated Copper Surfaces. J. Electrochem. Soc. **2021**, 168, 121507.

(42) Chiter, F.; Costa, D.; Maurice, V.; Marcus, P. Adsorption of 2-mercaptobenzimidazole Corrosion Inhibitor on Copper: DFT Study on Model Oxidized Interfaces. J. Electrochem. Soc. **2020**, 167, 161506.

(43) Kozlica, D. K.; Kokalj, A.; Milošev, I. Synergistic effect of 2-mercaptobenzimidazole and octylphosphonic acid as corrosion inhibitors for copper and aluminium – An electrochemical, XPS, FTIR and DFT study. Cor. Sci. **2021**, 182, 109082.

(44) Zhang, Z.; Wang, Q.; Wang, X.; Gao, L. The influence of crystal faces on corrosion behavior of copper surface: First-principle and experiment study. Appl. Surf. Sci. **2017**, 396, 746–753.

(45) Sun, G.; Kürti, J.; Rajczy, P.; Kertesz, M.; Hafner, J.; Kresse, G. Performance of the Vienna ab initio simulation package (VASP) in chemical applications. J. Mol. Struct. THEOCHEM **2003**, 624, 37–45.

(46) Kresse, G.; Hafner, J. Phys. Rev. B **1993**, 47, 558.

(47) Kresse, G.; Furthmüller, J. Efficiency of ab-initio total energy calculations for metals and semiconductors using a plane-wave basis set. Comput. Mater. Sci **1996**, 6, 15–50.

(48) Kresse, G.; Furthmüller, J. Efficient iterative schemes for ab initio total-energy calculations using a plane-wave basis set. Phys. Rev. B **1996**, 54, 11169–11186.

(49) Kresse, G.; Joubert, D. From ultrasoft pseudopotentials to the projector augmented-wave method. Phys. Rev. B **1999**, 59, 1758–1775.

(50) Blöchl, P. E. Projector augmented-wave method. Phys. Rev. B **1994**, 50.

(51) Perdew, J. P.; Chevary, J. A.; Vosko, S. H.; Jackson, K. A.; Pederson, M. R.; Singh, D. J.; Fiolhais, C. Atoms , Molecules , Solids , and Surfaces: Applications of the Generalized Gradient Approximation for Exchange and Correlation. Phys. Rev. B **1992**, 46.

(52) Perdew, J. P.; Burke, K.; Ernzerhof, M. Generalized Gradient Approximation Made Simple. Phys. Rev. Lett. **1996**, 77.

(53) Methfessel, M.; Paxton, A. T. High-precision sampling for Brillouin-zone integration in metals. Phys. Rev. B **1989**, 40.

(54) Grimme, S. Semiempirical GGA-Type Density Functional Constructed with a Long-Range Dispersion Correction. J. Comput. Chem. **2006**, 27.

(55) Kittel, C. Introduction to Solid State Physics, 7th ed.; Wiley Sons, New York, 1996.

(56) Chiter, F.; Nguyen, V. B.; Tarrat, N.; Benoit, M.; Tang, H.; Lacaze-Dufaure, C. Effect of van der Waals corrections on DFT-computed metallic surface properties. Mater. Res. Express **2016**, 3, 046501.

(57) Monkhorst, H. J.; Pack, J. D. Special points for Brillonin-zone integrations. Phys. Rev. B **1976**, 13.

(58) Koch, H. P. Absorption Spectra and Structure of Organic Sulphur Compounds. J. Chem. Soc. Part III **1949**, 401–108.

(59) Chesick, J. P.; Donohue, J. The Molecular and Crystal Structure of 2-Mercaptobenzothiazole. Acta Cryst. B **1971**, 27, 1441–1444.

(60) Rai, A. K.; Singh, R.; Singh, K. N.; Singh, V. B. FTIR, Raman spectra and ab initio calculations of 2-mercaptobenzothiazole. Spectrochim. Acta A **2006**, 63, 483–490.

(61) Mohamed, T. A.; Mustafa, A. M.; Zoghaib, W. M.; Afifi, M. S.; Farag, R. S.; Badr, Y. Reinvestigation of benzothiazoline-2-thione and 2-mercaptobenzothiazole tautomers: Conformational stability, barriers to internal rotation and DFT calculations. J. Mol. Struct.: THEOCHEM **2008**, 868, 27–36.

(62) Li, W.; Liu, M.; Liu, L.; Zhao, H. Thermodynamic functions for solubility of 2-mercaptobenzothiazole in eleven pure organic solvents at temperatures from 273.15 K to 318.15 K and mixing properties of solutions. J. Chem. Thermodynamics **2017**, 112, 196–203.

(63) Kokalj, A.; Peljhan, S.; Finšgar, M.; Milošev, I. What Determines the Inhibition Effectiveness of ATA, BTAH, and BTAOH Corrosion Inhibitors on Copper? J. AM. CHEM. SOC. **2010**, 132, 16657–16668.

(64) Trasatti, S.; Doubova, L. M. Crystal-Face Specificity of Electrical Double-Layer Parameters at Metal/Solution Interfaces. J. Chem. Soc., Faraday Trans. **1995**, 91, 3311–3325.

(65) Peljhan, S.; Koller, J.; Kokalj, A. The Effect of Surface Geometry of Copper on Adsorption of Benzotriazole and Cl. Part I. J. Phys. Chem. C **2014**, 118, 933–943.

(66) Mathew, K.; Sundararaman, R.; Letchworth-Weaver, K.; Arias, T. A.; Hennig, R. G. Implicit solvation model for density-functional study of nanocrystal surfaces and reaction pathways. J. Chem. Phys. **2014**, 140, 084106.

(67) Mathew, K.; Kolluru, V. S. C.; Mula, S.; Steinmann, S. N.; Hennig, R. G. Implicit self-consistent electrolyte model in plane-wave density-functional theory. J. Chem. Phys. **2019**, 151, 234101.

(68) Tomasi, J.; Mennucci, B.; Cammi, R. Quantum mechanical continuum solvation models. Chem. Rev. **2005**, 105, 2999–3093.

(69) Marenich, A. V.; Cramer, C. J.; Truhlar, D. G. Universal solvation model based on solute electron density and a continuum model of the solvent defined by the bulk dielectric constant and atomic surface tensions. J. Phys. Chem. B **2009**, 113, 6378.

(70) Kovačević, N.; Kokalj, A. The relation between adsorption bonding and corrosion inhibition of azole molecules on copper. Cor. Sci. **2013**, 73, 7–17.

(71) `https://echa.europa.eu/`.

(72) Kokalj, A.; Peljhan, S. Density Functional Theory Study of ATA, BTAH, and BTAOH as Copper Corrosion Inhibitors: Adsorption onto Cu(111) from Gas Phase. Langmuir **2010**, 26, 14582–14593.

(73) Lennartz, M. C.; Atodiresei, N.; Müller-Meskamp, L.; Karthäuser, S.; Waser, R.; Blügel, S. Cu-Adatom-Mediated Bonding in Close-Packed Benzoate/Cu(110)-Systems. Langmuir 2009, 25, 2, 856–864 **2009**, 25, 856–864.

(74) Milanova, E.; Ellis, S.; Sitholé, B. Aquatic toxicity and solution stability of two organic corrosion inhibitors: 2-mercaptobenzothiazole and 1,2,3-benzotriazole. Nord. Pulp Pap. Res. J **2001**, 16, 215–218.

Preprint accepted for publication in Corrosion Science, 2022.
https://doi.org/10.1016/j.corsci.2022.110658

Tables

Table 2: Adsorption energy (eV/molecule) for different adsorption modes and monolayer densities of thione (MBTH), radical (MBT°) and charged (MBT$^-$) thiolate species on the Cu(110) surface. Values were calculated with the thione form as reference. Values in brackets are the adsorption energy normalized to an unit area (eV/nm^2). Perpendicular (P) or tilted (T) orientation of the molecular plane and ratio of Cu atoms of the topmost plane involved in bonding are also indicated.

	Monolayer density (molecule/nm2)				
Adsorption modes	0.61	1.22	2.45	3.68	Figures
MBTH: -S -S	-1.96(-1.19) P	-1.95(-2.68) P	-1.97(-4.83) P All Cu occupied	-1.92(-7.06) T All Cu occupied	Fig.2(a) and (b)
MBTH: -S -NH	1.90 P	-1.89 P	-1.96 P Half Cu occupied	-1.85 P $\frac{2}{3}$ Cu occupied	Fig.2(c) and (d)
MBT°: -S -S	-1.96 P	-1.97 P	-2.09 P All Cu occupied	-2.06 T All Cu occupied	Fig.3(a) and (b)
MBT°: -S -N	-2.28(-1.39) P&T	-2.31(-2.82) P&T	-2.31(-5.66) P&T $\frac{2}{3}$ Cu occupied	-2.09(-7.69) P All Cu occupied	Fig.3(c) and (d)
MBT$^-$: -S -N	-2.52(-1.54)	-2.32(-2.83)	-1.98(-4.85)	-1.46(-5.37)	

Table 3: Vacancy formation energy (eV) for Cu atoms bonded to thione and thiolate species with different adsorption modes and monolayer densities on the Cu(110) surface. Bonding of the Cu atom is indicated in brackets. The value of 0.33 eV calculated for the bare Cu(110) surface is taken as the reference.

Adsorption modes	Low monolayer density (2.45 molecule/nm^2)	High monolayer density (3.68 molecule/nm^2)
Thione: -S -S	0.33 (free Cu) 0.60 (Cu–S_{exo}) 0.33 (Cu–S_{endo})	— 0.61/0.50 (Cu–S_{exo}) 0.52 (Cu–S_{endo})
Thione: -S -NH	0.33 (free Cu) 0.60 (Cu–S_{exo}) 0.40 (Cu–NH)	— 0.60/0.68 (Cu–S_{exo}) 0.50 (Cu–NH)
Thiolate: -S -N	0.33 (free Cu) 0.65/0.80 (Cu–S_{exo}) 0.95 (Cu–N)	— 0.60/0.70 (Cu–S_{exo}) 0.58/1.08 (Cu–N)

Preprint accepted for publication in Corrosion Science, 2022.
https://doi.org/10.1016/j.corsci.2022.110658

Figures

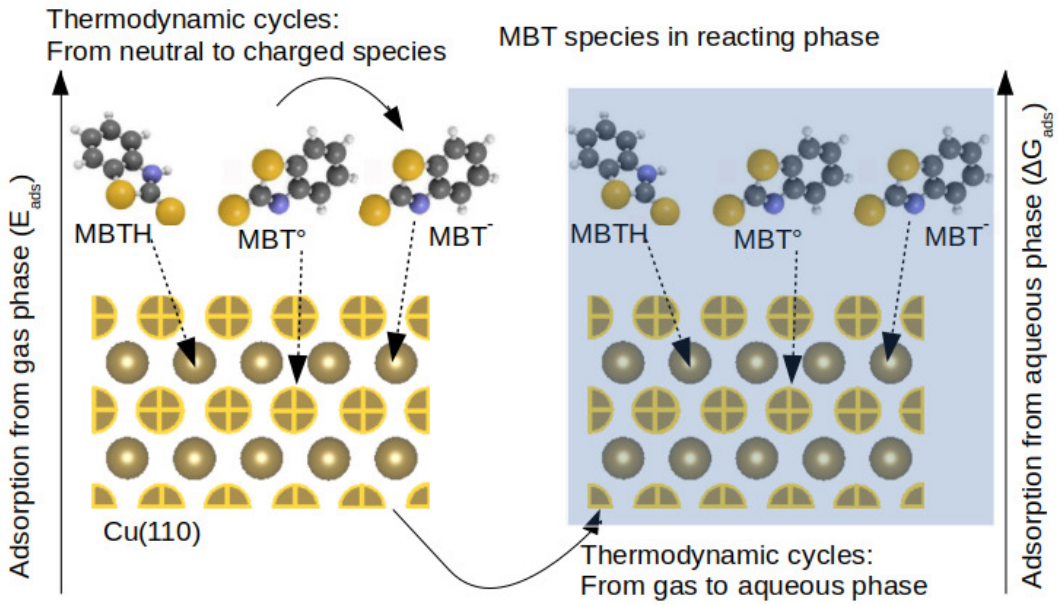

Figure 1: Adsorption modes of the different MBT species in reacting phase considered for interaction with the Cu(110) surface: adsorption of neutral and charged species, and from gas to aqueous phase, using a thermodynamic cycle.

Preprint accepted for publication in Corrosion Science, 2022.
https://doi.org/10.1016/j.corsci.2022.110658

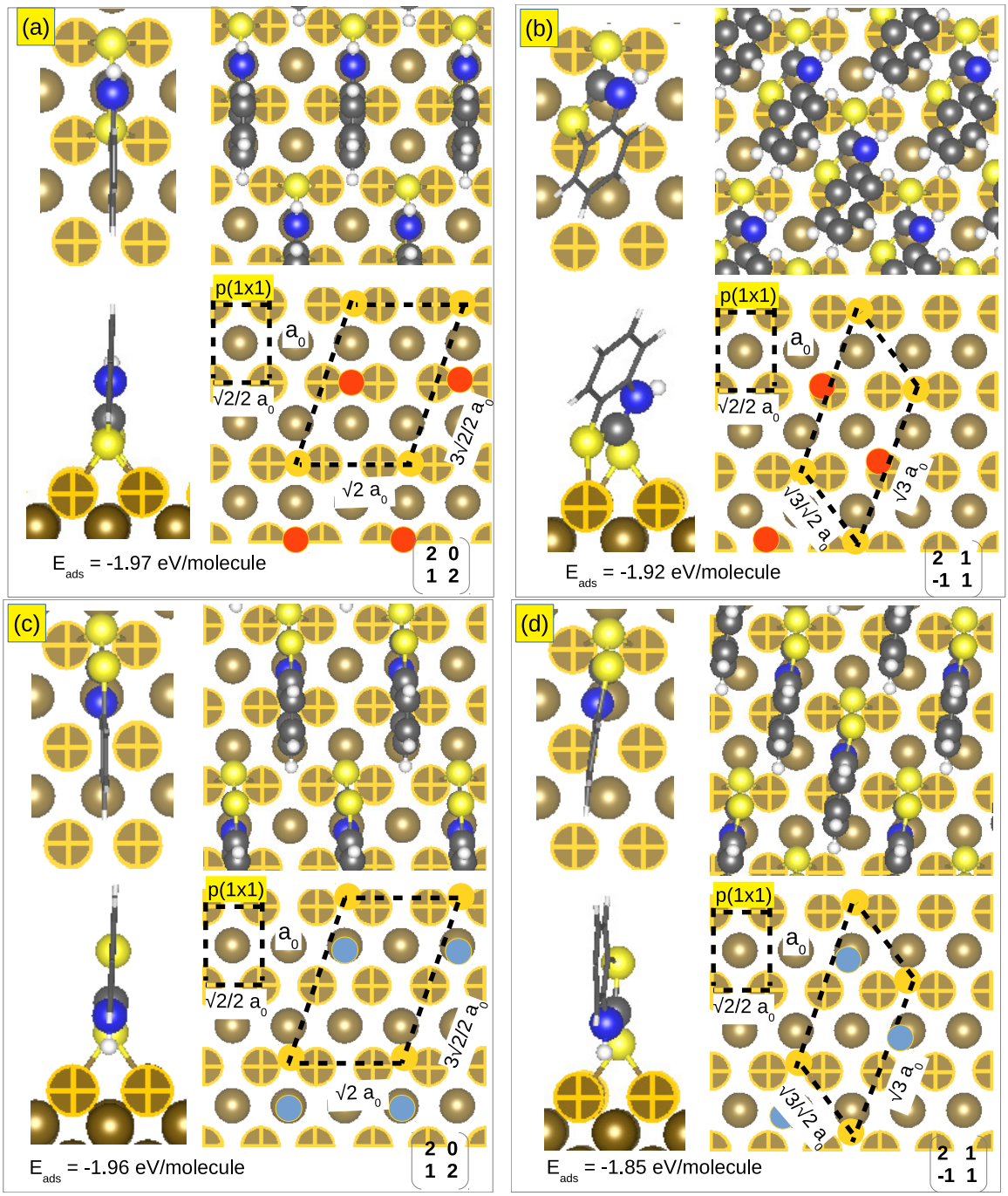

Figure 2: The most stable adsorption configurations of MBTH thione on Cu(110): (a) and (b) -S -S adsorption mode; (c) and (d) -S -NH adsorption mode; (a) and (c) monolayer density of 2.45 molecules/nm^2; (b) and (d) monolayer density of 3.68 molecules/nm^2. For each snapshot, the left panel shows the top and side views, the right panel shows the full organic layer and network lattices. Golden: copper under surface; hatched: copper surface; yellow: sulfur; blue: nitrogen; grey: Carbon.

Preprint accepted for publication in Corrosion Science, 2022.
https://doi.org/10.1016/j.corsci.2022.110658

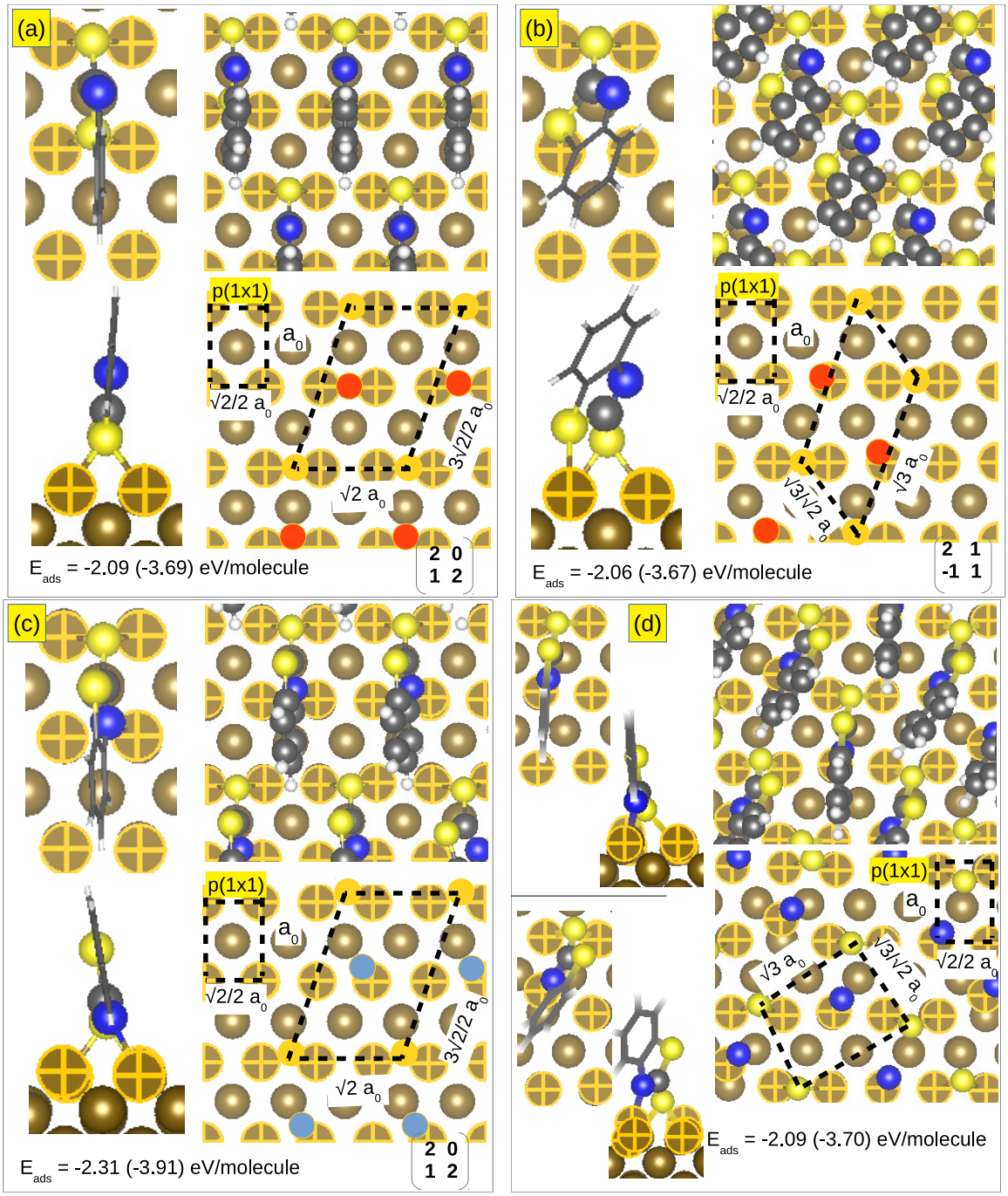

Figure 3: The most stable adsorption configurations of MBT° thiolate on Cu(110): (a) and (b) -S -S adsorption mode; (c) and (d) -S -N adsorption mode; (a) and (c) monolayer density of 2.45 molecules/nm^2; (b) and (d) monolayer density of 3.68 molecules/nm^2. For each snapshot, the left panel shows the top and side views, the rht panel shows the full organic layer and network lattices. In (d) top and side views for the non reconstructed and reconstructed copper surfaces are shown. Golden: copper under surface; hatched: copper surface; yellow: sulfur; blue: nitrogen; grey: Carbon.

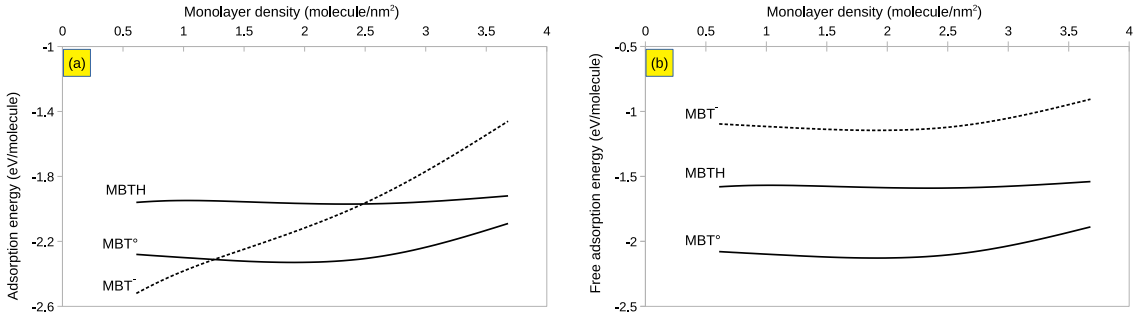

Figure 4: Variation of adsorption energies of MBT conformers on Cu(110) surface with density of organic film: (a) in gas phase (E_{ads}) and (b) in aqueous solution ($\Delta G_{\text{ads}}^{(\text{aq})}$).

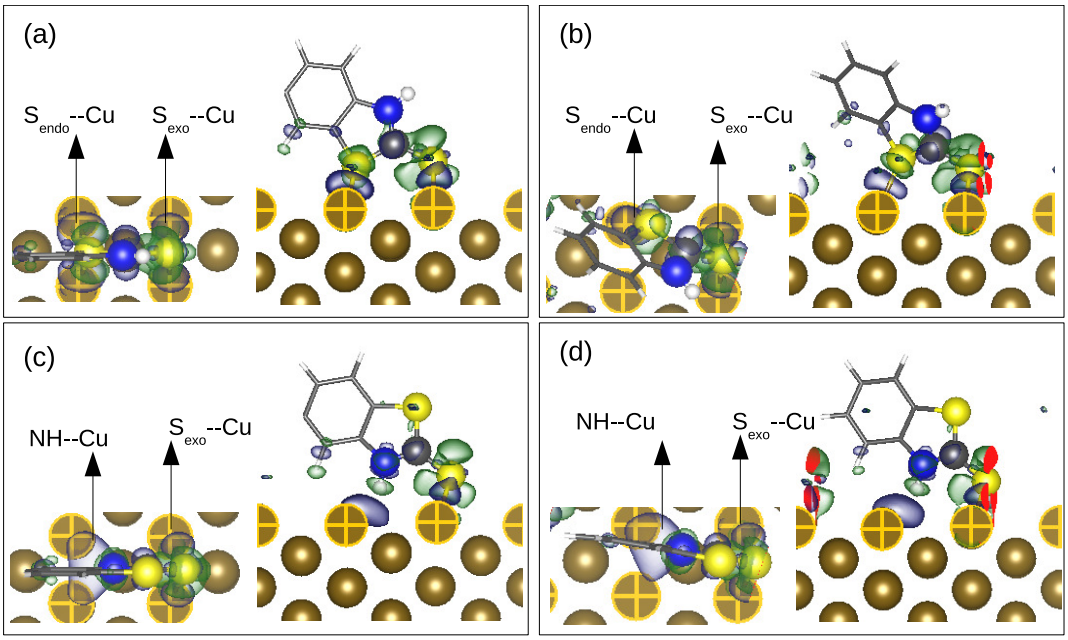

Figure 5: Top and side views of the charge density difference analysis plotted with an isosurface of ± 0.0004 e/Å^3 for MBTH thione adsorbed on Cu(110): (a) and (b) -S -S adsorption mode; (c) and (d) -S -NH adsorption mode ; (a) and (c) monolayer density of 2.45 molecules/nm^2; (b) and (d) monolayer density of 3.68 molecules/nm^2. Blue and green colors correspond to accumulation and depletion of charge density, respectively.

Preprint accepted for publication in Corrosion Science, 2022.
https://doi.org/10.1016/j.corsci.2022.110658

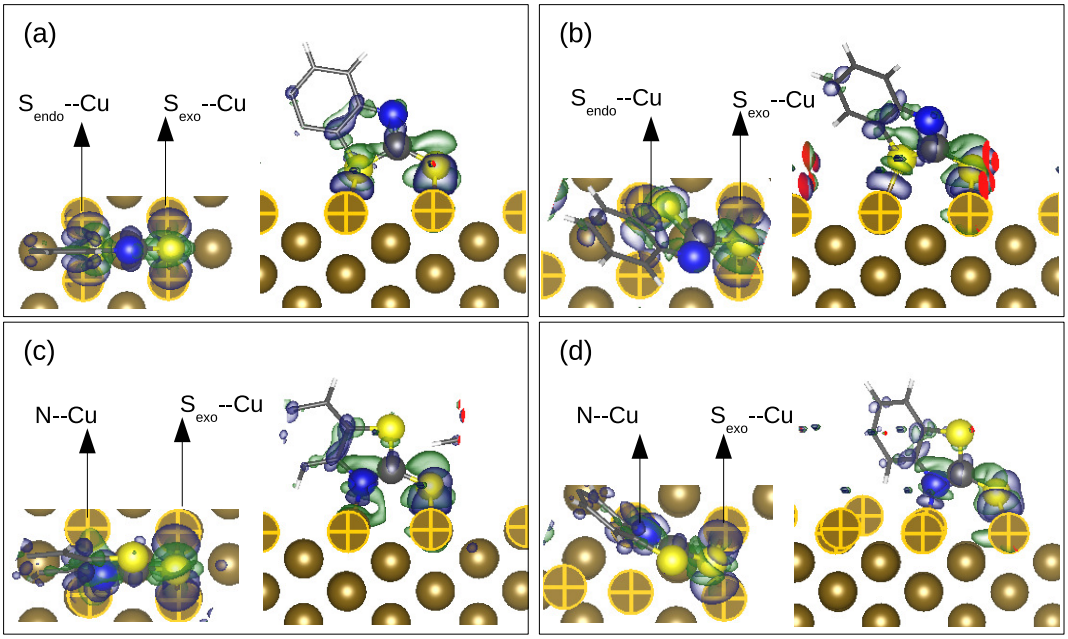

Figure 6: Top and side views of the charge density difference analysis plotted with an isosurface of ± 0.0004 e/Å^3 for MBT° thiolate form adsorbed on Cu(110): (a) and (b) -S -S adsorption mode; (c) and (d) -S -N adsorption mode; (a) and (c) monolayer density of 2.45 molecules/nm^2; (b) and (d) monolayer density of 3.68 molecules/nm^2. Blue and green color correspond to accumulation and depletion of charge density, respectively.

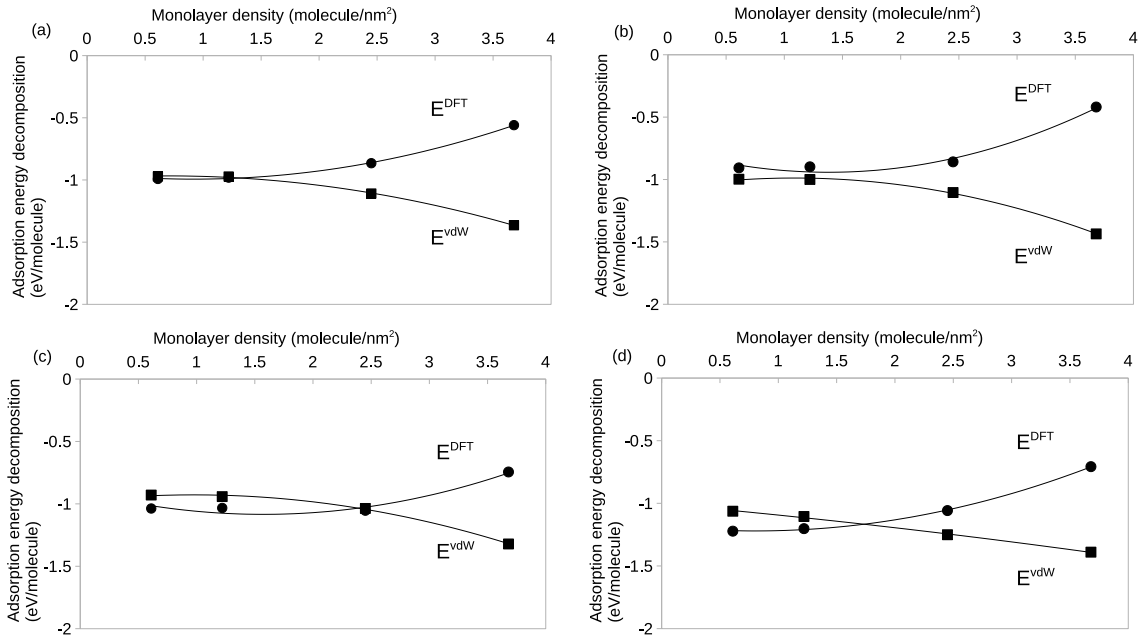

Figure 7: The adsorption energy decomposition (terms E^{vdW} and E^{DFT}) with density of organic film for MBTH thione and MBT° thiolate adsorbed on Cu(110). For MBTH thione: (a) -S -S adsorption mode; (b) -S -NH adsorption mode. For MBT° thiolate: (c) -S -S adsorption mode; (d) -S -N adsorption mode.

Preprint accepted for publication in Corrosion Science, 2022.
https://doi.org/10.1016/j.corsci.2022.110658

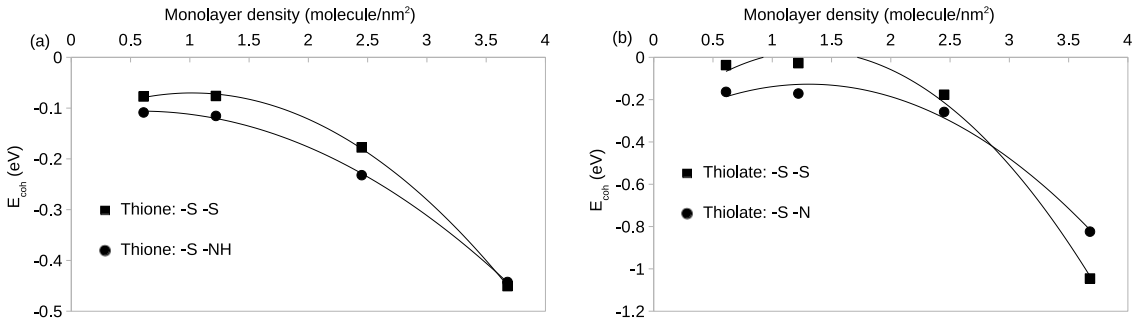

Figure 8: Variation of the cohesion energy with density of organic film: (a) MBTH thione in -S -S and -S -NH adsorption modes; (b) MBT° thiolate in -S -S and -S -N adsorption modes.

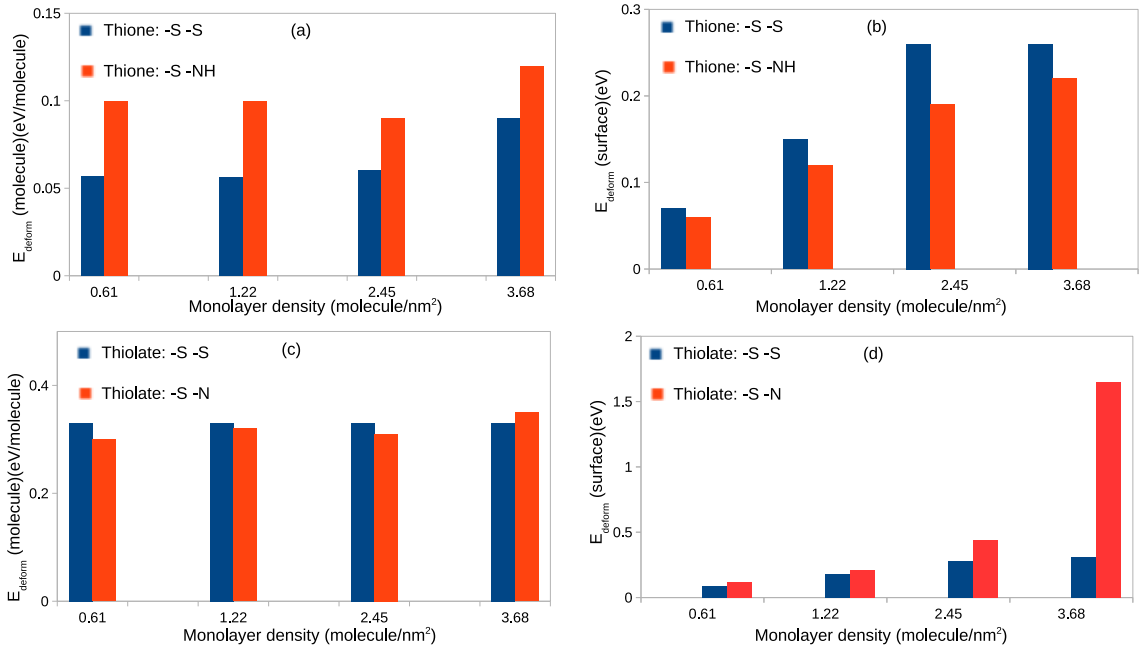

Figure 9: Variation of molecule (left column) and surface (right column) deformation energies with density of organic film, for MBTH thione (a) and (b) and for MBT° thiolate (c) and (d) adsorbed on Cu(110).

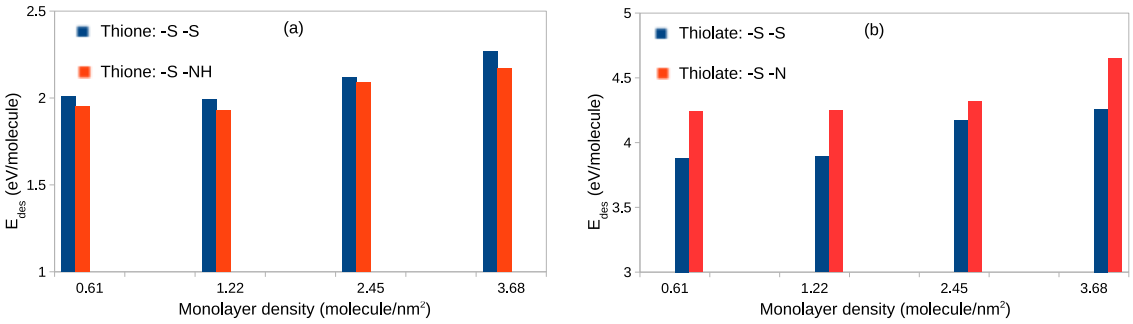

Figure 10: Variation of desorption energy with density of organic film on Cu(110): (a) MBTH thione in -S -S and -S -NH adsorption modes; (b) MBT° thiolate in -S -S and -S -N adsorption modes.